Independent Component Analysis for the Detection of In-Vivo Intrinsic Signals from an Optical Imager of Retinal Function.

Eduardo S. Barriga[1, 2], Marios Pattichis[2], Michael Abramoff[3], Dan T'so[4], Young Kwon[3], Randy Kardon[3], and Peter Soliz[5]

[1]ORION International Technologies, Albuquerque, NM, [2]University of New Mexico, Albuquerque, NM, [3]University of Iowa, Iowa City, IA, [4]SUNY Upstate University, Syracuse, NY, [5]VisionQuest Biomedical, Albuquerque, NM.

ABSTRACT

To overcome the difficulty in detection of loss of retinal activity, a functional-Retinal Imaging Device (f-RID) was developed. The device, which is based on a modified fundus camera, seeks to detect changes in optical signals that reflect functional changes in the retina. Measured changes in reflectance in response to the visual stimulus are on the order of 0.1% to 1% of the total reflected intensity level, which makes the functional signal difficult to detect by standard methods because it is masked by other physiological signals and by noise.

In this paper, we present a new Independent Component Analysis (ICA) algorithm used to analyze the video sequences from a set of experiments with different patterned stimuli from cats and humans. The ICA algorithm with priors (ICA-P) uses information about the stimulation paradigms to increase the signal detection thresholds when compared to traditional ICA algorithms. The results of the analysis show that we can detect signal levels as low as 0.01% of the total reflected intensity. Also, improvement of up to 30dB in signal detection over traditional ICA algorithms is achieved. The study found that in more than 80% of the in-vivo experiments the patterned stimuli effects on the retina can be detected and extracted.

1. INTRODUCTION

In the field of ophthalmology, visual field testing (perimetry) is the gold standard for detection and monitoring progression of diseases such as glaucoma. Perimetry is a functional test of the patient's vision intended to detect defects on the visual field map. Unfortunately, perimetry remains a subjective test that requires the patient to make important judgments during the test that can be clouded by anxiety, fatigue, or lack of concentration. As a result, the sensitivity of this test is poor. Investigators have found that over fifty percent loss of ganglion cells is necessary to detect loss of function with perimetry [1]. Low sensitivity and poor repeatability are frequently observed in areas where anatomical damage has occurred.

functional-Retinal Imaging Device (f-RID) has been developed in an attempt to improve the objectiveness of the test and the sensitivity for detection of damage and change over time [2]. The F-RID measures the increase or decrease in retinal reflectance due to changes in retinal metabolism thought to be a result of blood oxygen uptake and capillary response due to neural activity resulting from visual stimulation of the photoreceptors in the human retina. The functional measurements are stored as optical recordings (videos). The reflectance measurements recorded in these videos are a mixture of the signal that reflects the neuronal activity (functional signal) and signals related to background unknown sources and noise. Given that measured functional changes in intensity due to visual stimulus are on the order of 0.1% to 1% of the background signals, it is difficult to extract the functional response using standard methods, such as first frame subtraction and averaging. Our goal is to extract the functional signal that is masked by other signals present during the process of retinal stimulation.

In recent years, ICA has been applied to many biological related problems such as electroencephalography (EEG) data analysis [3, 4], and electrocardiogram (ECG) data analysis [5]. Schiessl et al. applied ICA techniques to isolate changes on the brain cortex of a macaque monkey due to visual stimulation [6, 7]. ICA has been applied extensively to detect

functional brain activation in functional magnetic resonance imaging (fMRI) experiments[8]. The authors of this paper have previously reported on the application of ICA techniques to isolate the changes produced in the retina due to visual stimulation [9-12]. This paper extends our prior work by incorporating prior information on the visual stimuli into the ICA algorithms.

This paper is organized as follows: Section 2 presents a description of the f-RID and its biological principles. In section 3 the ICA methods are discussed. Section 4 presents the results of the comparison of the ICA methods using synthetic and live data. In section V, a discussion of the results is presented.

2. MATERIALS AND DATA COLLECTION

A. Biological Principles

As early as 1949, Hill and Keynes linked the activity of the nerve cells with changes in their optical properties [13]. In 1986, Grinvald et al. showed that changes in the optical properties of the tissue could be used to study the functional architecture of the cortex [14]. Villringer and Chance used near-infrared light to assess brain activity in humans non-invasively through the skull.

Functional changes in the optic disc and radial papillary capillaries due to stimulus of the retina have been attributed as changes in hemodynamics. Riva and associates [15, 16] have investigated flicker-evoked responses of human optic nerve and subfoveal choroidal blood flow. Although optical techniques are mentioned, their approach is based on laser blood flow measurements. Because the retina is highly vascularized and has a particularly high rate of oxidative metabolism, altered hemodynamics can be observed as changes in reflection and absorption cause by a stimulus. Previous studies have demonstrated a visual stimulus-induced change in blood flow and oxygenation [15, 17, 18]. The choroidal circulation in the outer retina is known to have a very high flow rate and a small arteriovenous oxygen saturation difference. In contrast, the retinal circulation nourishing the inner retina, including the ganglion cells has a much slower flow rate and a high arteriovenous saturation difference [19]. This dichotomy suggests that any optical signal due to oximetry will be dominated by the retinal circulation component, and hence more closely reflect the function of the inner retina activity which is of most interest in clinical applications.

Bizheva, et al.[20] used a high resolution functional optical coherence tomography (fOCT) imager to measure *in-vitro* local changes in tissue reflectivity due to physiological changes in dark-adapted retinas as a result of light stimulation. fOCT scans were acquired from these *in-vitro* retinas synchronously with electrical recordings before, during, and after light stimulation. Their research clearly shows the stimulus-related changes in the retinal reflectivity profile of the inner and outer segments of the photoreceptor layer and the plexiform layers. This group conducted experiments to show, through pharmacological inhibition of photoreceptor function, that the origin of the observed optical changes is the altered physiological state of the retina evoked by the light stimulus. These studies have shown conclusively that reflectivity in the inner retina of a vertebrate does result from light stimulation.

Using a fMRI technique, blood oxygenation level-dependent (BOLD) [21], Duong, et al. [22] have measure deoxyhemoglobin changes that are brought about by visual stimuli. Changes in regional deoxyhemoglobin content can be visualized in BOLD images. When the retina is stimulated, retinal blood flow increases disproportionately to overcompensate for the stimulus-induced lowering of the hemoglobin saturation resulting from the neural activity. Duong showed convincingly that hemoglobin saturation conditions do indeed result in a functional signal in the retina. Unfortunately, fMRI is not a convenient clinical device for ophthalmology.

These findings motivate the development of a functional imager of the retina that can, using an instrument suitable for the clinical environment, directly measure spatially resolved retina function. The F-RID measures the increase or decrease in retinal reflectance due to changes in retinal metabolism thought to be a result of blood oxygen uptake and capillary response due to neural activity resulting from visual stimulation of the photoreceptors in the human retina.

B. The Functional-Retinal Imaging Device (F-RID)

The F-RID is a non-invasive imaging device that measures changes in retinal reflectance that result from changes in the blood oxygen saturation and blood volume when patterned stimuli is applied to the subject's retina [2]. The hypothesis is that a visual stimulus causes the retina to alter its level of blood volume and the ratio of oxygenated hemoglobin (HbO) to deoxygenated hemoglobin (Hb). This has the effect of altering the spectral reflectance characteristics of the retina and in turn results in a change in the reflected intensity of the image in the stimulated area.

Fig. 1 illustrates the operation the F-RID. A continuous interrogation light with wavelength in the red-near infrared wavelengths (780-850 nm) is projected onto the subject's retina. Simultaneously, a stimulus pattern at a green wavelength (550nm) is projected onto the subject's retina. The reflected energy from the retina is then filtered by the beam splitter, which only allows only the interrogation light to be transmitted to the digital recording camera. Kardon and associates have previously presented a detailed description of the system [2].

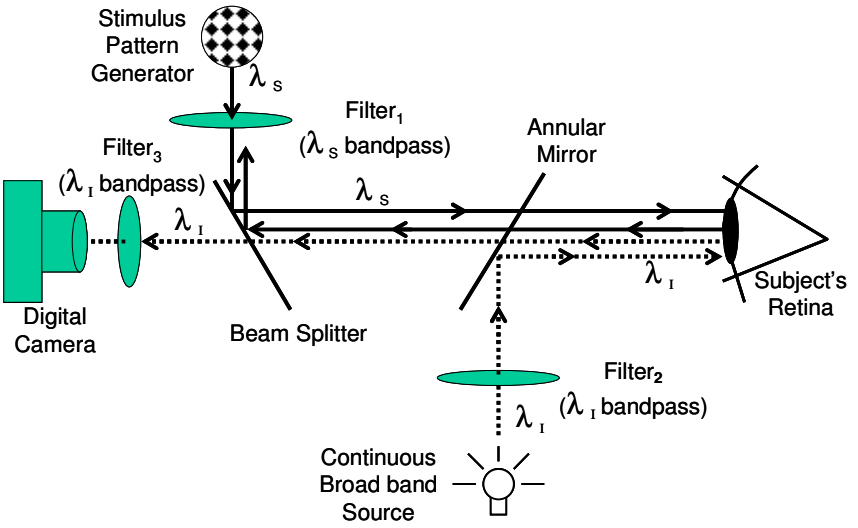

Fig. 1. Optical layout of the F-RID. The interrogation light, at λ_I = 780-850 nm, illuminates the retina and is reflected back to the imaging device. The spatial changes in reflected intensity are affected by the hemodynamics in the retina. The stimulus is presented to the retina at λ_S = 550 nm. The reflected stimulus light is filter out before reaching the imaging camera at filter $_3$.

The experimental data were collected from a cat by Ts'o [23]. To avoid artifacts due to eye movements, the cat is anesthetized and immobilized prior to the experiments. A single experiment (epoch) consists of 20 frames of 144 by 192 pixels each, at a frame rate of 2 Hz for a total recording time of 10 s. The stimulus paradigm consists of a checkered

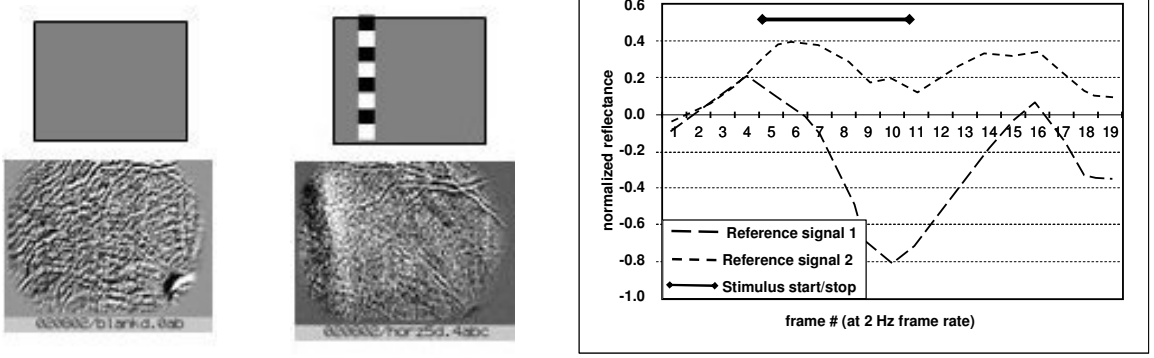

(a) **(b)** **(c)**

Fig. 2. (a) Pre-stimulated retina in the interrogation spectral band. (b) Stimulus pattern and response of a live experiment using a cat. (c) Signals for a region within the dark stimulated area (between pixels 21-40 in the x-axis) and within the bright stimulated area (between pixels 41-60 in the x-axis).

pattern with alternating polarity (counter-flickering at 1-20 Hz). Each experiment starts with a baseline (pre-stimulus) measurement where for the first 2 s the stimulus is turned off. This is followed by a 3 s period of stimulation and 5 s of recovery (post-stimulus). The bar-shaped, counter-flickering, checkered stimulus can be applied to a vertical or horizontal region of the retina. Fig. 2a is an image of the pre-stimulated (baseline) retina as measured in the interrogation band (near infrared). Fig. 2b shows a vertical counter-flickering stimulus bar with the corresponding measured reflectance of the infrared signal during the maximum functional response signal (about the 10^{th} frame). Fig. 2c presents the time plot of the functional response for the stimulated region. The region, which is in the dark response area of Fig 2b, is approximately at the second white stimulus box from the top. To the right of the same box another region is sampled that shows a negative response (white region) just outside the stimulated region.

3. INDEPENDENT COMPONENT ANALYSIS

Let $X = [x_1(t)\, x_2(t) \ldots x_n(t)]^T$ be a set of observed random variables and assume that they come from the linear mixture of the components $S = \left[s_1(t)\, s_2(t) \ldots s_n(t) \right]^T$ by a mixing matrix A, as in

$$X = A\, S. \qquad (1)$$

Then independent component analysis consists of estimating both A and S using only the observations in X and the assumption that the source signals are statistically independent [24].

In this paper we present an ICA algorithm using prior information about the visual stimulus. This algorithm will be compared to three different ICA algorithms: Infomax [25]; which uses maximum likelihood estimation (MLE) to extract the sources that give the highest probability for the observations; JADE [26] a popular ICA algorithm that consists on using higher-order cumulant tensors; and SOBI [27] a method that incorporates time structure in the estimation of the sources.

ICA Using Priors

In the basic ICA model, no information is available about the original sources or the mixing matrix. But in many cases, some prior information about the system is known and it can be incorporated into the unmixing process. This will certainly be our case here since we know the onset and offset of the visual stimuli which indirectly gives us information about the mixing matrix. Calhoun et al. [28] used prior information on fMRI experiments to determine spatial locations and temporal information about the extracted sources.

For this work, a simplified version of Calhoun's algorithm was used. The Infomax algorithm is modified so that we incorporate prior information at each update cycle. The Bell-Sejnowski form of the Infomax algorithm is used, where the negative log-likelihood function for the unmixing matrix is given by:

$$f(W) = -\left[N \log|W| - \sum_{i,j} \cosh(W X) - N M \log(\pi) \right], \qquad (2)$$

where N and M are the dimensions of the data. The gradient for this function is given by:

$$\Delta W = -\left[N \left(W^T\right)^{-1} - \tanh(W X)\, X^T \right]. \qquad (3)$$

Using the log-likelihood function and the gradient we can use an optimization method to obtain an estimate of the mixing matrix. We used the BFGS method for unconstrained optimization. At each iteration, a normalized cross-

correlation measure between the estimated mixing matrix and the prior of the mixing matrix is performed. If the correlation is lower than a tolerance value t then the estimated mixing matrix is updated as:

$$W^i = W^i + c\left(W_p^i - W^i\right) \qquad (4)$$

where W^i is the i-th column of the estimated mixing matrix, W_p^i is the prior for that column and c is the confidence value (between 0 and 1) for the prior information. For $c = 0$ there will be no change in the estimated mixing matrix, while for $c = 1$ the estimated mixing matrix will be transformed completely into the prior.

4. SYNTHETIC DATA SIMULATIONS

In the ICA literature there have been many efforts to quantify the performance of the algorithms [29]. Most of these efforts are confined to one-dimensional data sets, with few focusing on 2-dimensional data and almost none on the three-dimensional video applications. It is therefore important to explore the performance of the selected ICA algorithms in realistic simulations of both general spatiotemporal data-sets as well as more specific data sets that are constructed from actual optical imaging data from the F-RID device. In this section we present results from both a synthetic video simulation and a hybrid simulation using live data and synthetic stimuli.

A. Synthetic Video Simulations

A synthetic video is generated by mixing three images (sources) with a mixing matrix that contains the temporal structures of two sinusoids and a smoothed negative step function.

1) Experimental Setup

Fig. 2 gives a graphical scheme of the mixture of the signals. The mixing matrix contains the temporal signal with 40 samples each. The temporal signals are:

- Sinusoid #1: Period is 20 samples; peak-to-peak amplitude is 2 (units are arbitrary).
- Sinusoid #2: Period is 10 samples; peak-to-peak amplitude is 2.
- Smoothed negative rectangular function: This function is formed as a union of two. The amplitude of this signal varies in three different experiments: 10 %, 5%, and 1% of the peak-to-peak amplitude of the sources.

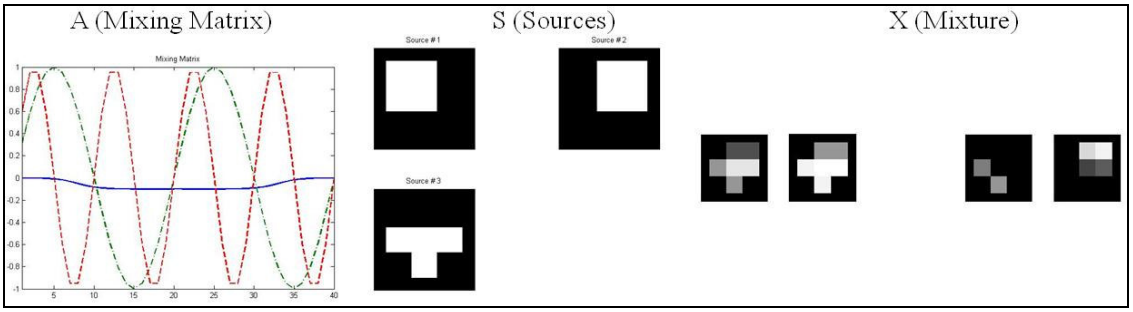

Figure 2. Experimental setup for the synthetic video simulation: Mixing matrix (left), sources (middle), and mixtures

The spatial signals are three 16-by-16 pixels binary images. The bright regions in those images (middle of Fig. 2) have a value of 1. The bright regions in the images were designed in such a way that when the linear mixture is performed using the mixing matrix, all mixing possibilities are covered. There are three regions which contain one temporal signal, three regions which are a mixture of two temporal signals and one region which contains a mixture of all the temporal signals described before. In total there are 7 different regions plus the background. The spatial arrangement also covers all the

possible combinations of spatial mixing: (i) Three regions with one signal each, (ii) three regions with a mixture of two signals each, (iii) one region with a mixture of all the signals, and (iv) the background where no signal except noise is present.

The resulting mixture is a video with 40 frames (number of time points in the mixing matrix) and 256 pixels each frame. The video is input to the ICA matrix in a matrix form and the results of the estimation should give us the temporal structure (in the estimated mixing matrix) and the spatial structure (in the estimated sources). Noise is added in the simulations, ranging from 40dB to 0dB in 10dB intervals.

2) Synthetic Video Results

The results of the normalized cross-correlations between the estimated sources and estimated mixing matrices are shown in Figs. 3 and 4. The "temporal" results refer to the comparison of the columns of the mixing matrices while the "spatial" results refer to the comparison of the sources with their estimated counterparts.

Spatial results for the rectangular signal (Fig. 3) show an increase in the performance of the ICA-P compared to the traditional Infomax algorithm, but it is still 10% less accurate than JADE, especially for the 10% and 5% signals in the 40 to 20dB range.

The ICA-P achieves the best results in the temporal estimation of the rectangular signal in the video simulations. Fig. 4 presents the plots for the temporal estimation of the rectangular signal and it is clear how ICA-P matches the performance of JADE for high SNR and greatly improves the performance for low levels of SNR. These levels are where we had the most difficulty estimating the rectangular signal, especially when the signal is 1% of the peak-to-peak amplitude of the sinusoids.

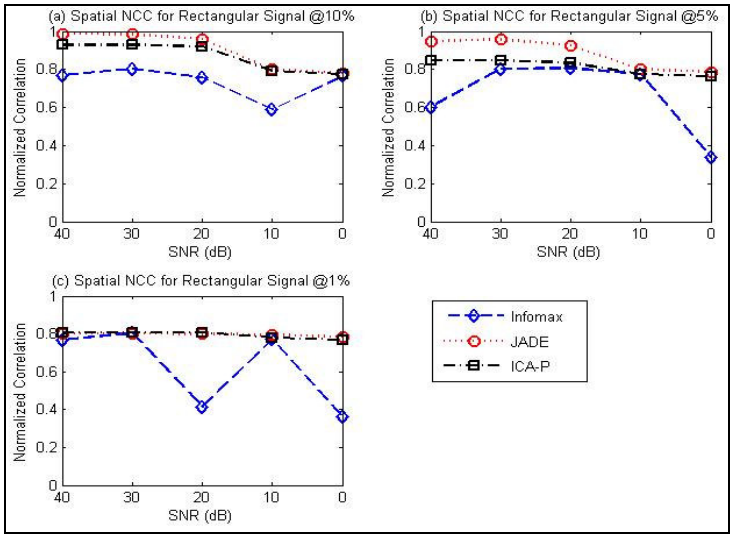

Figure 3. Spatial NCC results for the rectangular signal. Comparative results for JADE, Infomax, and ICA-P.

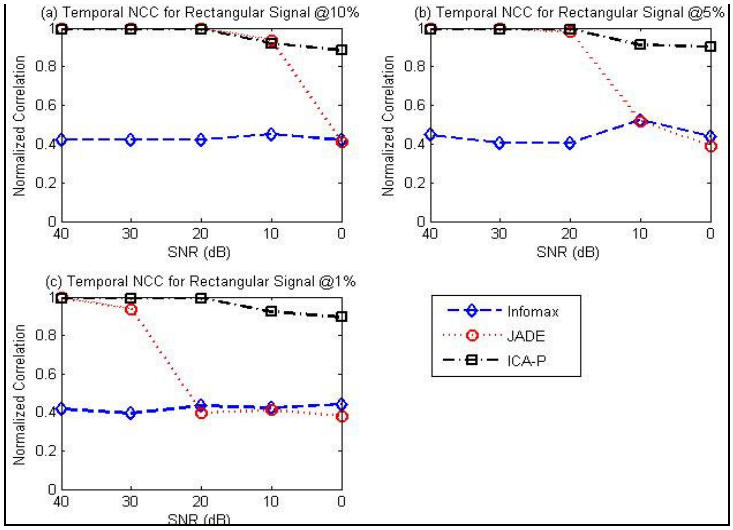

Figure 4. Temporal NCC results for the rectangular signal.

B. Hybrid Simulations

The next simulation involves both live data and synthetic stimulation. We use the F-RID recordings from an unstimulated cat retina and add synthetic stimuli at different of levels of signal-to-background ratio (SBR). The synthetic stimuli are obtained from actual recordings of stimulated cat retina and synthesized so they can be easily manipulated in our simulation.

1) Experimental Setup

To synthesize the stimuli, we used a live cat experiment recording that presented a clear response and extracted a spatiotemporal profile of the response change during the experiment. The resulting "stimulation video" was then averaged and filtered to produce a smooth response and normalized to unit variance so it can be manipulated to produce the desired level of simulated response.

In the hybrid simulation no noise is added to the mixture. Instead, the amplitude of the stimulus is controlled by the signal-to-background ratio (SBR), defined as:

$$SBR(dB) = 10\log_{10}\frac{\sigma_S^2}{\sigma_B^2} \qquad (5)$$

where σ_S^2 is the variance of the functional signal and σ_B^2 is the variance of the background.

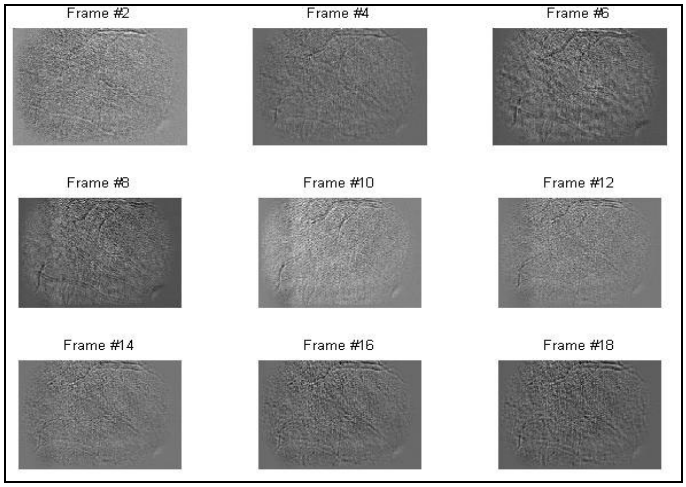

Figure 5. Sample frames from a hybrid video. Note the vertical synthetic stimulus on frames 8, 10, and 12.

Five videos were synthesized starting with the SBR ranging from 0 dB to -40 db at -10 dB intervals. Note that the more negative the SBR value, the lower the amplitude of the functional signal. A 0 dB SBR indicates that the variance of the functional signal is equal to the variance of the video, whereas a -30 dB SBR means that the variance of the functional signal is 0.1% of the variance of the video. Fig. 5 shows nine frames of a sample hybrid video at -20 dB SBR.

2) Hybrid Simulation Results

The results of the ICA algorithms were compared in the temporal and spatial domains. In the spatial domain, we correlated the sources as estimated by the ICA algorithms with a "reference frame," which is an image artificially generated by using a frame of pre-stimulated retina and the artificial stimulus response on top. For the temporal comparison, each row of the estimated mixing matrix was correlated with the modeled functional responses. A high correlation means that the estimated mixing matrix is following the time trace of the functional response expected due to visual stimulation.

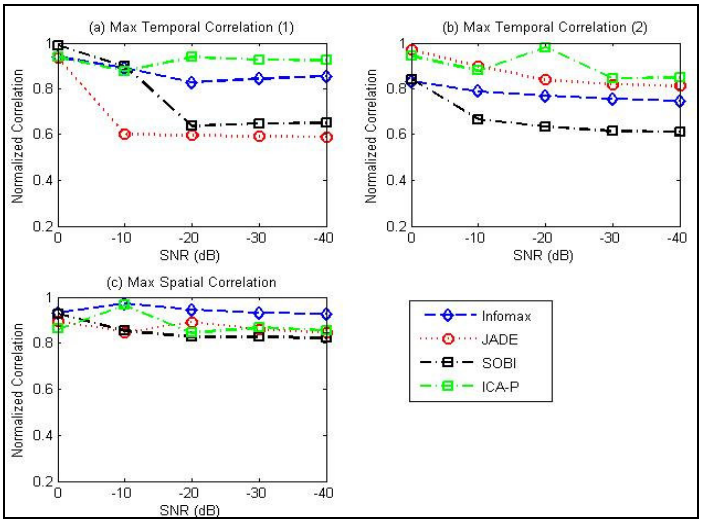

Figure 6. Temporal and spatial correlation results for live data plus synthetic stimulation experiments. (a) Temporal correlation results using the temporal reference 1. (b) Temporal correlation results using the temporal reference 2. (c) Spatial correlation results using the reference frame.

The application of the ICA-P algorithm in the hybrid simulation yields similar results as with the synthetic video simulations. Increased NCC values are observed in the temporal cases (Figs. 6a and 6b) and a decrease compared to the Infomax in the spatial case (Fig. 6c). Note that the priors represent information about the *mixing matrix*. Therefore, in the *spatial domain*, it is somewhat expected that we increase the performance in the temporal domain and decrease it in the

spatial domain. This is not a problem, since one of the most difficult parts in analyzing the data is recovering the correct temporal profile, and also we do not have (or use) priors in the spatial domain.

5. LIVE DATA ANALYSIS

The data set selected for the cat data analysis consists of 60 videos with four different types of stimulation. All the videos (epoch) have a duration of 10 seconds (s), with a frame rate of two frames per second (fps). The stimulus paradigm consists on of a checkered pattern with alternating polarity that is off for the first 2 s, representing the baseline (pre-stimulus), on for 3 s of stimulation, and 5 s of recovery (post-stimulus). The stimulus is applied in different spatial regions at multiple orientations. Our data is composed of 18 videos with vertical bar stimulation, 18 with horizontal bar stimulation, 3 with spot stimulation (The pattern is a small box), 3 with full field stimulation (the stimulus pattern covers the whole field of view) and 18 with no stimulation (for control purposes) for a total of 60 videos [23]. Cat data were analyzed using Infomax, JADE, SOBI, and ICA-P to estimate the spatiotemporal responses to visual stimulation.

A. Vertical Stimulation

A series of vertical stimulation patterns are applied to the cat's retina. Out of 18 experiments with vertical stimuli, using ICA we were able to see that 15 show a response that can be related to the optical stimulation (83%). Fig. 7 shows the estimated sources for four different vertical stimulation profiles as estimated with four different ICA algorithms. Note the similarities between the estimated sources in the live data and the estimated sources of the hybrid simulations in the previous section. The hybrid simulations have now a correspondence with live data and from the results obtained in those simulations we are confident in the correct estimation of signal variations as small as 0.1% (-30 dB SBR) of the overall data variance.

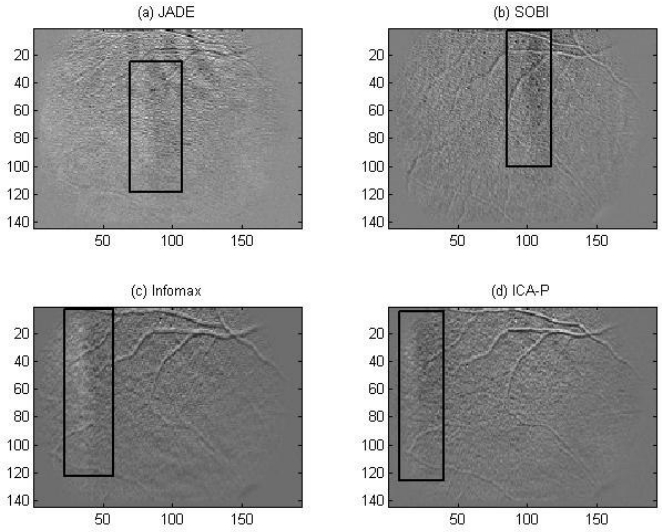

Figure 7. Spatial responses to vertical stimuli as extracted by: (a) JADE (b) SOBI (c) Infomax (d) ICA-P.

The boxed regions in Fig. 7 show the response to the visual stimulus as estimated by the ICA algorithms. Fig. 8 shows the temporal responses corresponding to these estimated sources. The dashed grids in those figures correspond to the onset and offset of the visual stimuli. Corresponding to the grids, positive (JADE) and negative (SOBI, Infomax, and ICA-P) responses are observed in the plots. We have to remark that the sign of the response is irrelevant due to the ambiguity issue of the ICA algorithms.

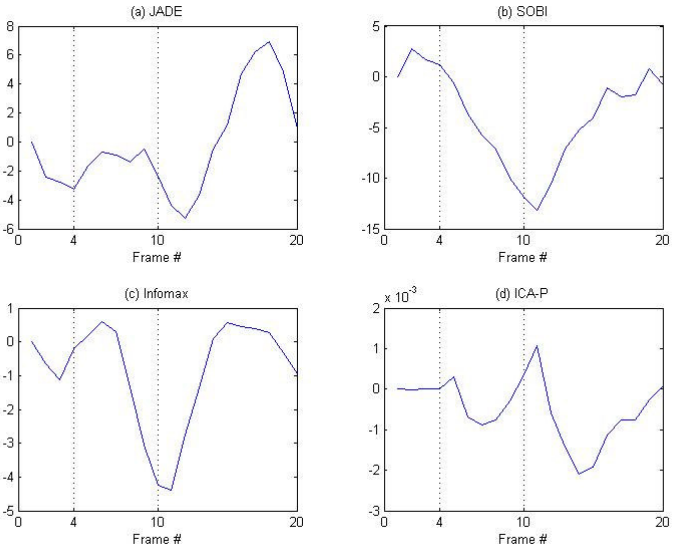

Figure 8. Temporal responses to vertical stimuli corresponding to the sources in Fig. 5.2. The Y-axis units are irrelevant due to the scaling issue on ICA.

From Fig. 7 we also note that the region where the response to the stimulus is seen is formed by two adjacent regions, one brighter and the other darker than the rest of the image. We have noted variations of this phenomenon in all cat videos, but

thus far there is not a satisfactory physiological explanation. Fig. 9 illustrates this phenomenon.

B. Horizontal Stimulation

A series of 18 experiments with a horizontal bar stimuli were performed for the same cat subject. In this case, from the 18 videos, we were able to extract signal in 16 of them (89%). An example of the estimated spatial responses is shown in Fig. 9. From Fig. 9 we note the same bright/dark pattern in the stimulated region.

C. Spot Stimulation

In this case the applied stimuli were little rectangular boxes. The responses to these stimuli are interesting because they do appear to be a combination of the bright/dark responses obtained with the vertical and horizontal stimuli. In this case we only show one of the estimated sources using the ICA-P along with its temporal response (Fig. 10). When there is a spot stimulation (small square) the left/bottom part of the square (lower triangle) forms the dark response region and the right/upper part of the square (upper triangle) forms the bright region. These spot responses appear as if the responses of the vertical and horizontal stimuli were somehow combined, where the directions of the horizontal and vertical directions were added into this diagonal response (See Fig. 11.)

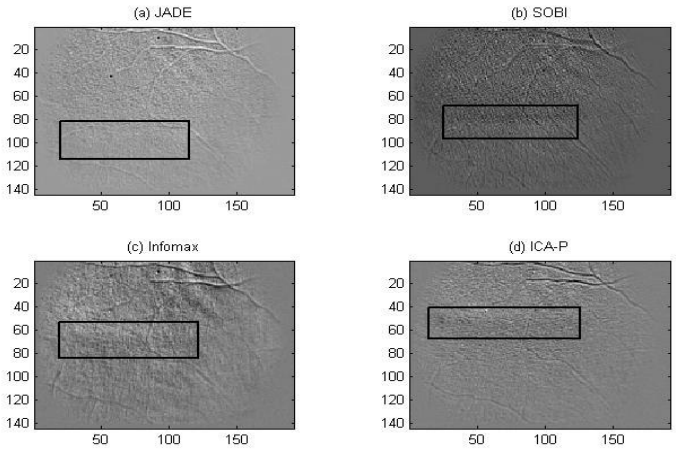

Figure 9. Spatial responses to horizontal stimuli as extracted by: (a) JADE (b) SOBI (c) Infomax (d) ICA-P.

6. DISCUSSION

For the cat experiments, it is clear that, no matter which stimulation condition occurred, visual stimulation evoked a very similar time course in the activated area. The signal changes started immediately after stimulus presentation and reached their peak in about 5 s.

These simulations have provided us with an improved understanding of the limits of what ICA algorithms can achieve, and how they can be improved. Our goal was to detect functional responses on the order of 0.1% (-30dB) of the total reflected signal. Our results showed how four ICA algorithms; JADE, Infomax, SOBI, and ICA-P produced estimates of the functional signals that were highly correlated with our reference signals.

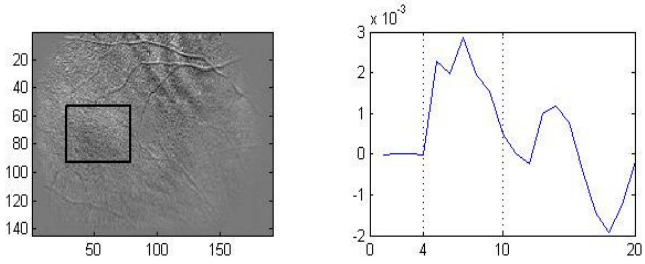

Figure 10. Spatial (left) and temporal (right) responses a spot stimuli as extracted with the ICA-P.

For the performance of ICA-P in the 3-dimensional simulations, we note significant improvement over conventional ICA algorithms. The results of the temporal correlations for the synthetic video simulations (Fig. 4) showed an improvement of up to 30 dB in SNR while detecting the small (1%) rectangular signal when compared to the best performer of the conventional algorithms (JADE). The results on the hybrid simulations also showed an improvement in the temporal correlations of about 0.05 in absolute normalized cross-correlation. These results demonstrate the power of introducing prior information about the temporal structure of the experiments.

Significant improvement over the Infomax algorithm (in which the ICA-P is based) has been achieved in the synthetic simulations based on physiological data (Fig. 4). Moreover, the ICA-P outperformed conventional ICA algorithms for up to 30 dB, proving to be a powerful tool for the analysis of complex biological signals. In the problem of signal detection, the requirement was to estimate signals as small as 0.1% of the total intensity of the images, and we have achieved detection for signals as small as 0.01% (-40 dB SBR) in the hybrid data simulations.

When studying the live cat data recordings we note several interesting results. First, it is clear that, as a result of the stimulation, two adjacent regions of contrasting reflectance are created. In the case of the vertical stimulation, the dark response region, i.e. increased blood volume, is distal to the optic disc and to the left of the bright response region. When there is horizontal stimulation, the bright response region is on top of the dark response region. Most interestingly, when there is a spot stimulation (small square) the left/bottom part of the square (lower triangle) forms the dark response region and the right/upper part of the square (upper triangle) forms the bright region, as if the responses of the vertical and horizontal stimulations were additive. Another interesting result is the way the functional response changes the reflectance through time (See Fig. 8 a-d). At first when the stimulus is applied (frame 5) there is a slight increase in reflectance but then immediately it starts to decrease, to reach its negative peak between frames 10 to 12 (2 to 3 seconds after the start of stimulation). After this negative peak the signal goes back up to higher levels than the original ones to finally come back to the original state after the stimulus is turned off. These results are consistent with other hemodynamical processes observed in the brain using techniques such as functional magnetic resonance imaging (fMRI) and functional near infrared imaging (fNIR).

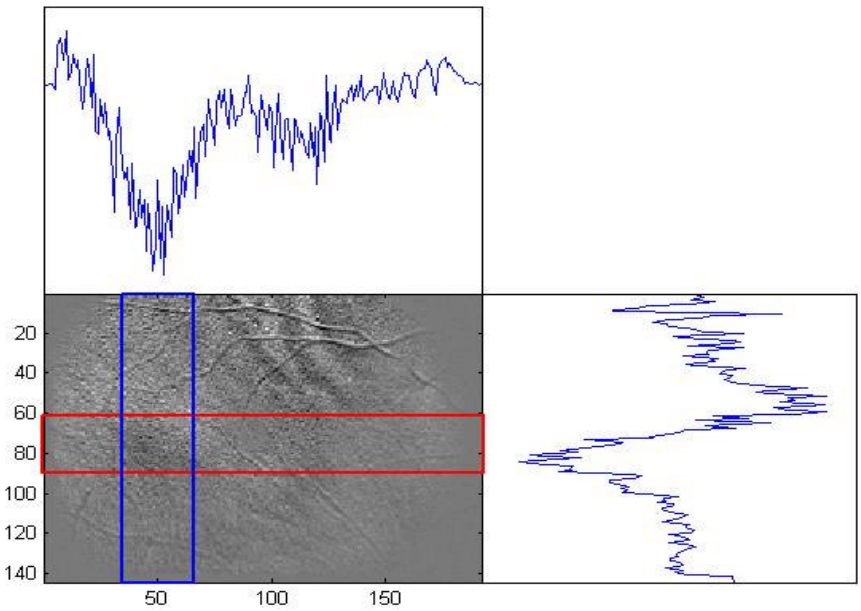

Figure 11. Line intensity profile for a spot stimulation experiment. The plot on the right corresponds to the average value in the X-direction from the blue box. The plot on top corresponds to the average value in the Y-direction from the red box.

7. CONCLUSIONS

We have demonstrated that non-invasive optical imaging of intrinsic signals in the retina reveals a spatial distribution of activity-dependent signals that is highly correlated with the pattern of visual stimulus presented to the retina. Our experimental data indicate that there are several different signals that differ in amplitude, time course, sign and spatial distribution. The most prominent signal has properties similar to the hemodynamic signals that we and others have previously reported in stimulus-activated mammalian sensory cortex. In particular these signals have a rise time of 1-3 seconds, amplitude of 0.01 to 0.1% and are negative in sign (representing a reflectance decrease). Further research will be required to determine the source and anatomic origins of these signals.

The experiments preformed by applying a synthetically generated functional response on top of an image of an unstimulated cat retina have provided us with information of the limits of detection achievable by the ICA algorithms. Our goal was to detect functional responses on the order of 0.1% (-30dB SBR) of the total reflected signal. This study will be more useful when analyzing data from human experiments, since in the human case the functional response is much lower than in the cat; because of more noise sources such as movement (the cat is anesthetized during the experiments, the human is not), lack of focus (the human subject cannot withstand long periods of stimulation) and the complexity of the human retina.

In conclusion, the f-RID has been demonstrated to produce a functional response in the cat retina due to visual stimulation. The analysis of the synthetic experiments has given us useful information in determining the threshold of stimulation that can be detected using the ICA algorithms. The analysis of these experiments will be useful to any signal processing application where spatiotemporal responses are present.

8. REFERENCES

[1] H. A. Quigley, G. R. Dunkelberger, and W. R. Green, "Retinal ganglion cell atrophy correlated with automated perimetry in human eyes with glaucoma," *Am J Ophthalmol*, vol. 107, pp. 453-464, 1989.

[2] R. Kardon, Y. H. Kwon, P. W. Truitt, S. C. Nemeth, D. Ts'o, and P. Soliz, "Optical imaging device of retinal function," *Ophthalmic Technologies XII. Proceedings of the SPIE*, vol. 4611, pp. 230-238, 2002.

[3] S. Makeig, A. J. Bell, T.-P. Jung, and T. J. Sejnowski, "Independent component analysis of electroencephalographic data," in *Advances in Neural Information Processing Systems*. Cambridge, MA: MIT Press, 1996, pp. 145-151.

[4] T.-P. Jung, C. Humpries, T.-W. Lee, M. J. McKeown, V. Iragui, S. Makeig, and T. J. Sejnowski, "Removing electroencephalographic artifacts by blind source separation," *Psychophysiology*, vol. 37, pp. 163-178, 2000.

[5] S. Choi, A. Cichocki, and S. Amari, "Fetal electrocardiogram data analysis via flexible independent component analysis," presented at The 4-th Asia-Pacific Conference on Medical & Biological Engineering (APCMBE'99), Seoul, Korea, 1999.

[6] I. Schiessl, M. Stetter, J. E. W. Mayhew, N. McLoughlin, J. S. Lund, and K. Obermayer, "Blind signal separation from optical imaging recordings with extended spatial decorrelation," *IEEE Transactions on Biomedical Engineering*, vol. 47, pp. 573-577, 2000.

[7] M. Stetter, I. Schiessl, T. Otto, F. Sengpiel, M. Hübener, T. Bonhoeffer, and K. Obermayer, "Principal Component Analysis and Blind Separation of Sources for Optical Imaging of Intrinsic Signals," *Neuroimage*, vol. 11, pp. 482-490, 2000.

[8] V. D. Calhoun and T. Adali, "Unmixing fMRI with Independent Component Analysis," *IEEE Engineering in Medicine and Biology*, vol. 25, pp. 79-90, 2006.

[9] E. S. Barriga, D. Y. Ts'o, M. S. Pattichis, and P. Soliz, "Independent component analysis for processing of retinal responses to patterned stimuli," *Engineering in Medicine and Biology Society, 2003. Proceedings of the 25th Annual International Conference of the IEEE*, vol. 1, pp. 1006-1009, 2003.

[10] E. S. Barriga, P. W. Truitt, M. S. Pattichis, D. Ts'o, R. H. Kwon, R. H. Kardon, and P. Soliz, "Blind source separation in retinal videos," *Medical Imaging 2003: Image Processing. Proceedings of the SPIE*, vol. 5032, pp. 1591-1601, 2003.

[11] E. S. Barriga, M. S. Pattichis, D. Y. Ts'o, Y. Kwon, R. Kardon, M. D. Abramoff, and P. Soliz, "Detection of low amplitude, in-vivo intrinsic signals from an optical imager of retinal function," *Ophthalmic Technologies XVI. Proceedings of the SPIE*, vol. 6138, pp. 66-77, 2006.

[12] E. S. Barriga, P. Soliz, and P. W. Truitt, "Functional signal detection in retinal videos," *The 2002 45th Midwest Symposium on Circuits and Systems, 2002. MWSCAS-2002.*, vol. 1, pp. I-443-6 vol.1, 2002.

[13] D. K. Hill and R. D. Keynes, "Opacity changes in stimulated nerve," *J Physiol*, vol. 108, pp. 278-281, 1949.

[14] A. Grinvald, E. Lieke, R. D. Frostig, C. D. Gilbert, and T. N. Wiesel, "Functional architecture of cortex revealed by optical imaging of intrinsic signals," *Letters to nature*, vol. 324, pp. 361-364, 1986.

[15] C. E. Riva, S. D. Cranstoun, J. E. Grunwald, and B. L. Petrig, "Choroidal blood flow in the foveal region of the human disc," *Investigative Ophthalmology and Visual Sciences (IOVS)*, vol. 35, pp. 4273-81, 1994.
[16] C. E. Riva, E. Logean, and B. Falsini, "Visually evoked hemodynamical response and assessment of neurovascular coupling in the optic nerve and retina," *Progress in Retinal and eye Research*, vol. 24, pp. 183-215, 2005.
[17] B. Falsini, C. E. Riva, and E. Logean, "Flicker-Evoked Changes in Human Optic Nerve Blood Flow: Relationship with Retinal Neural Activity," *Investigative Ophthalmology and Visual Sciences (IOVS)*, vol. 43, pp. 2309-16, 2002.
[18] R. A. Linsenmeier and L. Padnick-Silver, "Metabolic Dependence of Photoreceptors on the Choroid in the Normal and Detached Retina," *Investigative Ophthalmology and Visual Science (IOVS)*, vol. 41, pp. 3117-23, 2000.
[19] I. M. Hogeboom van Buggenum, G. L. Van der Heijde, G. J. Tangelder, and J. W. M. Reichert-Thoen, "Ocular Oxygen Measurement," *British Journal of Ophthalmology*, vol. 80, pp. 567-573, 1996.
[20] K. Bizheva, R. Pflug, B. Hermann, B. Povazay, H. Sattmann, P. Qiu, E. Anger, H. Reitsamer, S. Popov, J. R. Taylor, A. Unterhuber, P. Ahnelt, and W. Drexler, "Optophysiology: Depth-resolved probing of retinal physiology with functional ultrahigh-resolution optical coherence tomography," *Proceedings of the National Academy of Science of the USA*, vol. 103, pp. 5066-71, 2006.
[21] S. Ogawa, D. W. Tank, and R. Menon, "Intrinsic signal changes accompanying sensory stimulation: functional brain mapping with magnetic resonance imaging," *Proceedings of the National Academy of Sciences of the USA*, vol. 89, pp. 5951-5955, 1992.
[22] T. Q. Duong, S.-C. Ngan, K. Ugurbil, and S.-G. Kim, "Functional Magnetic Resonance Imaging of the Retina," *Investigative Ophthalmology and Visual Science (IOVS)*, vol. 43, pp. 1176-81, 2002.
[23] D. Y. Ts'o, H. Li, Y. H. Kwon, P. Truitt, and P. Soliz, "Intrinsic signal optical imaging of retinal responses to patterned stimuli," *Investigative Ophthalmology and Visual Sciences (IOVS) - ARVO abstract*, vol. 43, 2003.
[24] A. Hyvarinen, J. Karhunen, and E. Oja, *Independent component analysis*. New York: John Wiley, 2001.
[25] A. J. Bell and T. J. Sejnowski, "An information-maximization approach to blind separation and blind deconvolution," *Neural Computation*, vol. 7, pp. 1003-1034, 1995.
[26] J. Cardoso, "Infomax and maximum likelihood for blind source separation," *IEEE Signal Processing Letters*, vol. 4, 1997.
[27] A. Belouchrani, K. Abed-Meraim, J. Cardoso, and E. Moulines, "A blind source separation technique using second-order statistics," *IEEE Transactions on Signal Processing*, vol. 45, 1997.
[28] V. D. Calhoun, T. Adali, M. C. Stevens, K. A. Kiehl, and J. J. Pekar, "Semi-blind ICA of fMRI: A method for utilizing hypothesis-derived time courses in a spatial ICA analysis.," *Neuroimage*, vol. 25, pp. 527-38, 2005.
[29] A. Mansour, M. Kawamoto, and N. Ohnishi, "A survey of the performance indexes of ICA algorithms," *Proceedings of the 21st IASTED International Conference Modeling, Identification and Control (MIC '02)*, pp. 660-666, 2002.